IEEE Photonics Journal
An IEEE Photonics Society Publication

Open Access

Resonant Graphene-Based Tunable Optical Delay Line

Volume 7, Number 6, December 2015

D. Conteduca
F. Dell'Olio
C. Ciminelli
M. N. Armenise

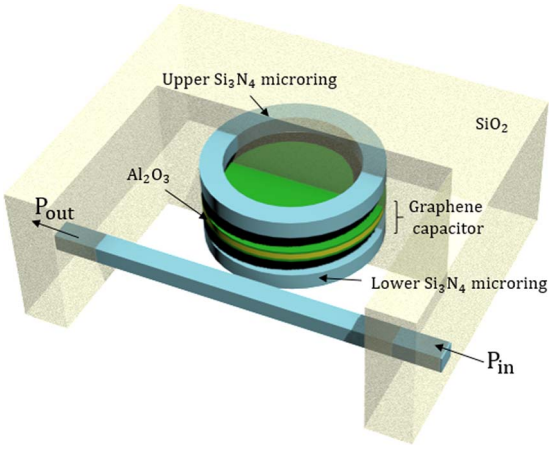

DOI: 10.1109/JPHOT.2015.2496245
1943-0655

Resonant Graphene-Based Tunable Optical Delay Line

D. Conteduca, F. Dell'Olio, C. Ciminelli, and M. N. Armenise

Optoelectronics Laboratory, Politecnico di Bari, 70125 Bari, Italy

DOI: 10.1109/JPHOT.2015.2496245

Manuscript received September 24, 2015; revised October 20, 2015; accepted October 23, 2015. Date of publication October 30, 2015; date of current version November 12, 2015. Corresponding author: C. Ciminelli (e-mail: caterina.ciminelli@poliba.it).

Abstract: The design of a new graphene-based continuously tunable optical delay line formed by two vertically stacked microring resonators coupled to a straight waveguide is proposed. High values of delay time ($\tau_g = 360$ ps) and a wide tuning range ($\Delta\tau_g = 230$ ps) have been calculated, due to the graphene sandwiched between the stacked ring resonators, which also provides an electrooptical tuning of the delay with low energy consumption ($E_{\text{switch}} = 3.4$ pJ) and fast switching time ($t_{\text{switch}} < 2$ ns). The ratio $\Delta\tau_g/A$ represents an important figure of merit (FOM) for optical delay lines. A value FOM $= 1.4 \times 10^{-1}$ ps/μm^2 has been calculated, which corresponds to an enhancement of about a factor 4 compared with the state-of-the-art of the integrated optical delay lines, also providing a switching time several times faster. Such performance, together with a small device footprint ($< 1.6 \times 10^3$ μm^2), gives a significant contribution to the state-of-the-art of optical delay lines, confirming the suitability of the graphene-based resonant cavity as a high-efficient optical delay line for applications in which fast tuning and wide range of tunability are required, e.g., phased array antennas.

Index Terms: Integrated optics devices, coupled resonators, nanomaterials.

1. Introduction

In recent years, optical delay lines have attracted strong interest due to their ability to control light propagation [1]. A delay time of few nanoseconds is necessary for several applications, such as the synchronization of optical data streams for the optical routing and data multiplexing in optical buffers [2], as well as for phased array antennas (PAAs) in optical beamformers. In particular, several advantages have recognized to optical delay lines for PAAs in comparison with the electronic beamformers, i.e., a relevant decrease of the beam squint with large aperture antennas and large arrays of elements, a wide bandwidth, reduced weight and size and the immunity to electromagnetic interference with low radio-frequency (RF) transmission loss. Such properties, typical of optical configurations, allow also the implementation of multi-task PAAs with multiple beamforming, required by modern radars and warfare systems [3]–[5]. Similar performance has been demonstrated in optical delay lines based on spiral patterns [6], Mach–Zehnder interferometer (MZI) switches [7], and optical fibers [8]. Their limit is related to a bulky configuration that makes difficult their integration and prevents reduced costs and low energy dissipation [9].

A more efficient on-chip integration due to a stronger light-matter interaction that enhances the manipulation of the dispersion properties of the light in resonant cavities has been proposed [10]. Resonant cavities have also typical small footprint, providing lower values of energy consumption

and fast switching time. However, such advantages have been achieved at the expense of lower values of the delay time, typically on the picosecond scale [11]. Longer delay time by cascading several resonant cavities in Side Coupled Integrated Spaced Sequence of Resonators (SCISSOR) and Coupled Resonator Optical Waveguide (CROW) configurations, have been proposed in the literature [12]. The former configuration includes several microring resonators each being side-coupled to a common waveguide, without any interaction from each other. The latter one is based on a cascade of several coupled microring resonators. Both configurations provide larger bandwidth and higher values of the delay time, improving the performance of the delay line with respect to those obtained by a single resonant cavity [13]. The maximum delay time achieved by the cascade of several resonant cavities in a SCISSOR configuration is $\tau_g \sim 1.2$ ns with a footprint of about 10^8 μm^2 [14], that is lower than that provided by spiral patterns or MZI switches. A smaller footprint $(= 9 \cdot 10^4$ μm$^2)$ has been also proposed with a maximum delay time $\tau_g = 500$ ps but with high optical loss (22 dB) [12]. High values of the time delay $(\tau_g = 800$ ps$)$ have been also obtained by using CROW configurations with a footprint of $5 \cdot 10^6$ μm^2 [11].

The range of tunability represents an important figure of merit for optical delay lines. In fact, several applications in optical communications require a large tuning range and also a fast tunability [15]. For this reason, a significant effort has been spent to search for new approaches and configurations capable of improving the tuning range. A broad tuning range has been calculated $(\Delta\tau_g \sim 500$ ps$)$ for a SCISSOR configuration with a footprint of 9×10^4 μm^2 [12], while $\Delta\tau_g \sim 300$ ps has been obtained with a smaller device footprint $(= 1.2 \times 10^4$ μm$^2)$ [16]. Photonic crystal (PhC) cavities have been also proposed to control and manipulate light [17]. Large delay time at nanosecond range has been obtained with coupled PhC cavities with large footprint of few mm^2 [18]. Also, a maximum delay time $\tau_g = 216$ ps and a tuning range $\Delta\tau_g = 200$ ps have been obtained with a smaller footprint of about 10^5 μm^2 [19].

The most used tuning approach is the thermo-optical one, where heating is used to change the resonance conditions, which is the easiest technique, even if the switching time is quite high $(> 10$ μs$)$ [20].

Unfortunately, such performance does not fulfill the requirements of fast tunability in few nanoseconds required to achieve broad steering angles for high efficiency phased array antennas.

Recently, the use of graphene in photonic and optoelectronic devices is increasingly growing, due to its unique electronic and optical properties, such as high mechanical strength, high flexibility and optimal thermal conductivity, high optical transparency and carrier mobility [21], [22]. Graphene-based optical devices suitable for optical communications, high-efficiency solar cells, low cost touch screens, and light-emitting diodes have been recently reported [23]–[29]. Graphene-based optical delay lines electro-optically tuned have been proposed recently with PhC cavities [30] and cascaded microring resonators in both SCISSORs and CROWs configurations. High values of maximum delay time $\tau_g = 200$ ps and $\tau_g = 250$ ps have been obtained with CROW and SCISSOR structures, respectively, with a footprint smaller than 10^5 μm^2. The most remarkable advantage of such cavities is related to a switching time of about 0.12 ns due to the electro-optic approach, five orders faster than typical values obtained with thermo-optic effect [31].

In this paper we present the design of a fast tunable optical delay line based on a resonant cavity formed by two vertically-stacked microrings among which is located a capacitor with graphene electrodes. The cavity provides a strong light control and manipulation, achieving a maximum delay time $\tau_g = 360$ ps, extinction ratio $ER \leq 23$ dB and a bandwidth $B > 1$ GHz with a small footprint of 1600 μm^2. The graphene allows a tunable behavior by applying a voltage < 5 V, which corresponds to a continuous tuning range $\Delta\tau_g = 230$ ps and an energy consumption $E_{\text{switch}} = 3.4$ pJ with a fast switching time $t_{\text{switch}} < 2$ ns. This performance confirms the high efficiency of the proposed graphene-based optical delay line to achieve fast beam steering of phased array antenna in optical beamformers, allowing a precise control of both signal shape and beam angle of the transmitted and received signals without any information loss [32], and for biomedical imaging, where fast switching is necessary to achieve a high repetition of the video frame of the order of few nanoseconds for real-time imaging of matter specimens [33].

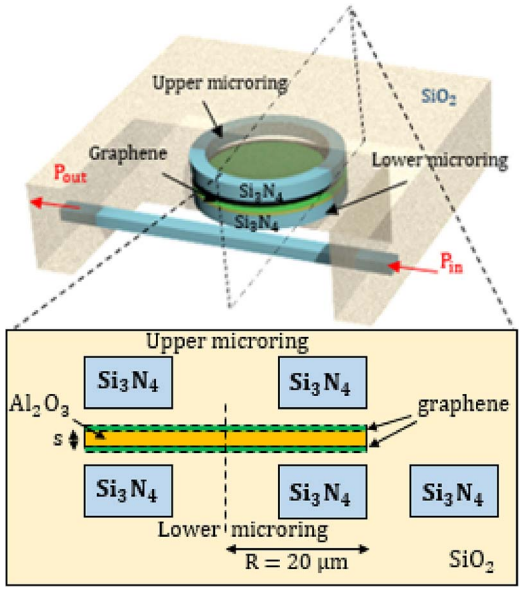

Fig. 1. Configuration of the graphene-based vertically stacked microring resonators.

2. Device Configuration and Operating Principle

The configuration of the graphene-based resonant cavity includes two vertically coupled microring resonators in Si_3N_4 ($n_{Si3N4} = 1.977$ at $\lambda = 1550$ nm) with a radius $R = 20$ μm. The lower microring is also coupled horizontally to a straight bus waveguide. The strip waveguide forming the rings and the bus has a width of 900 nm and a height of 644 nm [34]. A negligible coupling between the upper microring and the bus waveguide has been assumed. Two graphene monolayers with a thickness of 0.34 nm are sandwiched between the ring resonators and separated each other by a layer of Al_2O_3 ($n_{Al2O3} = 1.746$ at $\lambda = 1550$ nm) with a thickness $s = 10$ nm to form a capacitor. The graphene capacitor is placed between the two microring resonators to obtain a symmetrical structure of the device. The whole structure is surrounded by silica (SiO_2) ($n_{SiO2} = 1.444$ at $\lambda = 1550$ nm), as shown in Fig. 1 [35].

The cavity has been designed to let the quasi-TE fundamental mode resonate around 1550 nm. This device exhibits the basic features of a directional coupler with the excitation of supermodes and a periodic exchange of the optical power between the rings. Higher degrees of freedom in light manipulation have been demonstrated by considering the coupling since the values of the waveguide optical loss α and the horizontal and vertical coupling coefficients δ and k, respectively, strongly influence the cavity performance.

The graphene monolayers have been included in the device to tune the cavity performance, by applying a variable voltage. Optical losses and light phase in the cavity are indeed strongly affected by the voltage applied to the graphene layers.

A mature fabrication technique is available to realize the vertically-stacked ring resonators. The lower microring resonator in Si_3N_4 is defined through the typical processes of e-beam lithography and reactive ion etching (RIE) [37] and totally embedded in a silica layer by spinning a flowable oxide layer (followed by a thermal annealing in the oxygen ambient or by using the precursor tetraethocylane [38]). The Al_2O_3 can be grown by chemical vapor deposition (CVD) on the first graphene monolayer, placed on the silica layer with the same deposition technique as for the second graphene monolayer on the alumina, realizing the capacitor configuration with graphene layers and Al_2O_3 as electrodes and dielectric material, respectively. The pattern of the upper microring can be defined by the deposition of a Si_3N_4 layer with plasma enhanced-CVD or low pressure-CVD followed by the e-beam lithography and RIE. Finally, the whole cavity is fully embedded in the silica. The fabrication steps listed above provide a negligible change of

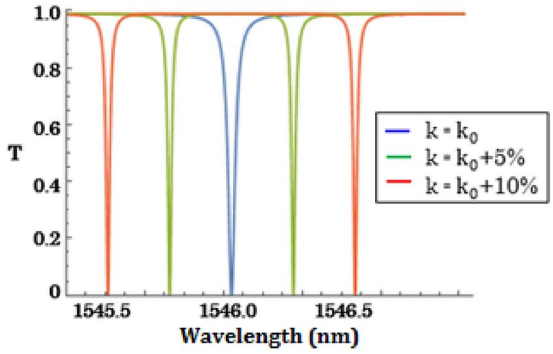

Fig. 2. Transmission spectra of the vertically stacked ring resonators for three values of k, without the graphene layers, assuming $\delta = 0.1$ and $\alpha = 0.12$ dB/cm [34].

the refractive index of SiO_2 and Si_3N_4 from the nominal values of both materials, as already confirmed in [37], where a perfect overlap between experimental and simulations results for the nominal values of the refractive indices was observed.

3. Numerical Results

The coupled mode theory (CMT) has been considered to study the propagation in the device without the graphene monolayers, as already discussed in [36]. The transfer function of the device is the following:

$$T(\lambda) = \left| t + \frac{\delta^2 e^{-i\beta L}\left[e^{-i\beta L} - \cos(kL)e^{L\frac{\alpha}{2}}\right]}{e^{L\alpha} + te^{-2i\beta L} - (1+t)e^{-i\beta L + L\frac{\alpha}{2}}\cos(kL)} \right|^2 \tag{1}$$

where t is the portion of field remaining in the bus waveguide and corresponds to $t^2 = (1-\gamma^2) - \delta^2$, where γ^2 is the coupler optical loss that we assumed equal to 1%, L is the cavity length $(= 2\pi R)$, and $\beta (= 2\pi n_{\text{eff}}/\lambda)$ is the propagation constant. Finite Element Method (FEM) simulations have been carried out to define the value of the effective index of the quasi-TE fundamental mode that propagates in the microring resonator. An optical loss $\alpha = 0.12$ dB/cm has been assumed, as already experimentally verified [34].

A resonance splitting has been observed in the cavity due to two supermodes with different propagation constant. The resonance splitting disappears at the degenerate condition, for which symmetric and antisymmetric supermodes have the same β value. Such condition has been obtained with $k = k_0 = \pi/L = 0.025\ \mu\text{m}^{-1}$, as shown in Fig. 2. Such coupling condition corresponds to a distance of 480 nm between the two microring resonators, as calculated by FEM simulations and the CMT approach.

The graphene conductivity has been calculated theoretically by taking into account both interband and intraband effects. The graphene has been modelled as an anisotropic layer, assuming the perpendicular relative permittivity $\varepsilon_\perp$ as constant, while the parallel component $\varepsilon_\parallel$ changes as a function of the voltage applied on the electrodes.

The real and imaginary parts of the optical conductivity of a graphene monolayer with a thickness $\Delta = 0.34$ nm are given by

$$\sigma_r = \sigma_0 \left[\frac{18 - \left(\frac{\hbar\omega}{\rho}\right)^2}{\pi 12\sqrt{3}}\right] \psi_r \kappa \tag{2}$$

$$\sigma_i = \left(\frac{\sigma_0}{\pi}\right)\left\{\frac{4\mu_c}{\hbar\omega}\left[1 - 2\left(\frac{\mu_c}{3\rho}\right)^2\right] - \left[1 - 2\left(\frac{\hbar\omega}{6\rho}\right)^2\right]\Upsilon\right\} \tag{3}$$

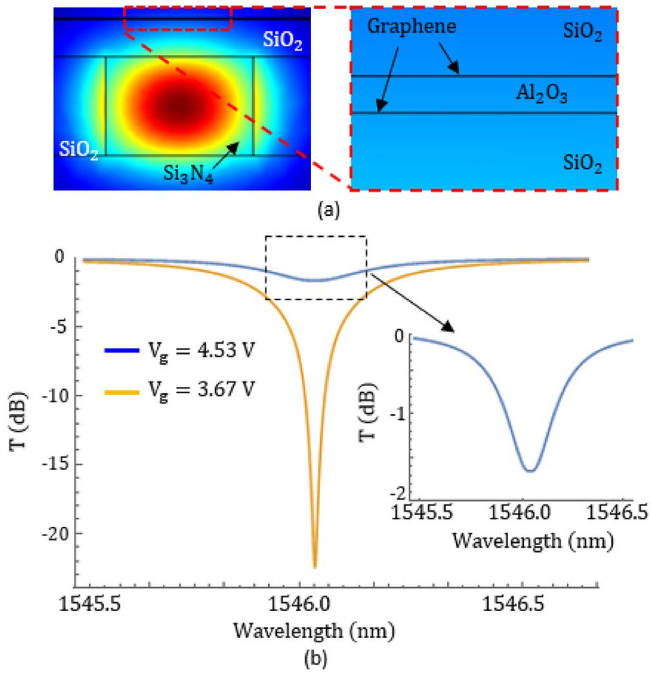

Fig. 3. (a) Mode distribution in Si_3N_4 waveguide with $V_g = 4.53$ V applied to the graphene monolayers. (b) Transmission spectra of the vertically stacked ring resonators with $\delta = 0.4$ as a function of V_g applied to the graphene layers.

where

$$\psi_r = \tanh\left(\frac{\hbar\omega + 2\mu_c}{4k_BT}\right) + \tanh\left(\frac{\hbar\omega - 2\mu_c}{4k_BT}\right) \tag{4}$$

$$\kappa = 4.6936 - 2.897\tanh\left(|\hbar\omega - 2\rho|^{0.546}\right) \tag{5}$$

$$\Upsilon = \log\left(\frac{|\hbar\omega + \mu_C| - \psi_i}{|\hbar\omega + \mu_C| + \psi_i}\right) \tag{6}$$

with

$$\Psi_i = 2k_BT\left[\tanh\left(\frac{|\hbar\omega + 2\mu_c|}{4k_BT}\right) - \tanh\left(\frac{|\hbar\omega - 2\mu_c|}{4k_BT}\right)\right] \tag{7}$$

and $\hbar$ the reduced Planck's constant, ρ is the hopping parameter assumed to be equal to 2.7 eV, k_B is the Boltzmann's constant, T is the temperature, μ_c the graphene chemical potential, and ω is the angular frequency.

We have assumed $\varepsilon_\perp = 1 + i16.39$, as for an undoped graphene monolayer, while the parallel relative permittivity of graphene is given by $\varepsilon_\parallel = 1 + i\sigma/\omega\varepsilon_0\Delta$, where σ is the complex conductivity, ε_0 the vacuum permittivity, i the imaginary unit, and Δ the graphene thickness [39].

Equation (8), shown below, describes the relationship between the graphene chemical potential and the voltage V_g applied across the electrodes:

$$\mu_c(V_g) = \hbar\nu_F\sqrt{\pi\frac{C'}{e}|V_g - V_0|} \tag{8}$$

where ν_F is the Fermi velocity, $C'(= \varepsilon_{Al2O3} \cdot \varepsilon_0/s)$ is the effective capacitance per unit area with $\varepsilon_{Al2O3} = 10$, e is the electron charge, and V_0 is the offset voltage for the natural doping $(= 0.8$ V$)$ [40]. A sharp decrease of the optical loss has been estimated in a range of μ_c around 0.4 eV,

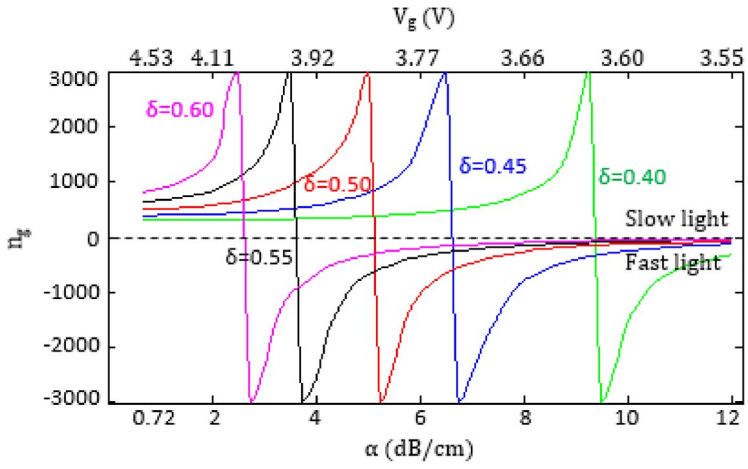

Fig. 4. Group index of the graphene-based cavity as a function of V_g and α for several values of δ. The best compromise between a broad linear tuning range of the group delay and a high value of the delay time has been achieved with $\delta = 0.4$.

while values that are almost constant have been obtained with $\mu_c \geq 0.53$ eV, confirming the results derived by applying the Kubo formalism [41]. A stronger energy consumption is required to obtain higher values of μ_c without any significant decrease of the optical loss. Therefore, $\mu_c = 0.53$ eV has been assumed as the best compromise to minimize the optical loss and the energy dissipation. This condition can be obtained by applying a voltage $V_g = 4.53$ V, according to (8).

The cavity performance has been first calculated assuming $V_g = 4.53$ V. We have assumed a slight change of 1% in the value of k from k_0, i.e., k equal to 0.02525 μm^{-1}, to improve the extinction ratio and also to preserve the degenerate mode condition.

An effective index $n_{\text{eff}} = 1.704 + i2.04 \cdot 10^{-6}$ has been calculated by FEM simulations with an applied voltage on graphene layers $V_g = 4.53$ V, which corresponds to $\beta = 2\pi \cdot n_{\text{eff}}/\lambda = 6.922 \cdot 10^6$ m^{-1}. A Q-factor of 6.4×10^3 at a resonating wavelength equal to $\lambda_R = 1546.05$ nm, a maximum delay time $\tau_g = 130$ ps, $ER = 1.7$ dB and a bandwidth $B = 7$ GHz have been calculated, assuming $\delta = 0.4$, as shown in Fig. 3.

Tuning of the delay time has been obtained by changing the voltage V_g across the graphene layers.

A detailed parametric analysis has been carried out to evaluate the optimal values of δ and α, that maximize the delay time and optimize the tuning range.

The coupling coefficient δ depends on the gap between the bottom ring and the bus waveguide and we consider it not tunable after the device fabrication, while α can be electrically tuned by changing V_g. The coupling coefficient k, which depends on the distance between the rings, has been kept constant at 0.02525 μm^{-1}. The minimum value of α is 0.72 dB/cm, which is obtained when $V_g = 4.53$ V, as discussed above. When V_g is reduced, α increases.

In Fig. 4, we have plotted the dependence of the device group index $n_g = \tau_g \cdot c/L = c/v_g$, ($v_g$ is the group velocity) on α at the resonance wavelength, for several values of δ in the range from 0.40 to 0.60. The slow-light regime is obtained for $n_g > 1$, which corresponds to $v_g < c$. Otherwise, the fast-light regime is provided when $n_g < 1$. Outside the δ range from 0.40 to 0.60 we have that for $\delta > 0.60$ only the fast-light regime is supported by the device while for $\delta < 0.40$ the resonance splitting condition, which provides different propagation constants of the symmetric and antisymmetric modes, has been observed. Under the latter conditions, small changes in the group delay have been observed at both resonances providing a narrow tuning range, which is not suitable for an efficient tunable delay line.

A slow light effect has been observed for all considered vales of δ $(0.40 < \delta < 0.60)$. First, the group index increases as α increases, then a sharp decrease of n_g is observed. After this abrupt

TABLE 1
Optical delay line performance

τ_{gmax}	360 ps
$\Delta\tau_g$	230 ps
E_{switch}	3.4 pJ
t_{switch}	< 2 ns
ER	23 dB

decrease, n_g again increases with α. The width of the range of α values suitable to use the device as slow-light-based delay line decreases as δ increases. For example, for the $\delta = 0.4$ the condition assuring the excitation of the slow-light regime is 0.72 dB/cm $< \alpha <$ 9.5 dB/cm, while for $\delta = 0.5$ the same condition is achieved for 0.72 dB/cm $< \alpha <$ 5.0 dB/cm.

In the slow light regime, the n_g dependence on α is nonlinear for $\delta = 0.45, 0.50, 0.55,$ and 0.60. For $\delta = 0.40$ we can observe that the n_g dependence on α is almost linear when 0.72 dB/cm $< \alpha <$ 7.8 dB/cm. Therefore, we have chosen as the operating condition $\delta = 0.40$ because a slow-light effect is provided with the broadest range of more linear behavior for the optical loss, as shown in Fig. 4. We have calculated that a gap between the bus waveguide and the lower microring $G = 240$ nm is necessary to satisfy such coupling condition $(\delta = 0.4)$. The method used for the bus/ring gap calculation based on the Coupled Mode Theory (CMT) is defined in [42] and [43].

As discussed above, a delay time $\tau_g = 130$ ps has been calculated with $V_g = 4.53$ V and $\alpha =$ 0.72 dB/cm. We have also obtained the maximum delay time $\tau_g = 360$ ps, with $\alpha = 7.8$ dB/cm, $\mu_c = 0.465$ eV, corresponding to $V_g = 3.67$ V. Under this condition, we have calculated $Q = 7 \times 10^3$, $ER = 23$ dB, and $B > 1$ GHz. Thus, by changing V_g from 4.53 V to 3.67 V, a continuous tuning range $\Delta\tau_g = 230$ ps is obtained.

This result achieved for our graphene-based device testifies a performance comparable with the CROW-based one reported in [12], but it is 30 times smaller.

The switching time and the energy consumption represent two important parameters to define the efficiency of the optical delay line. The most remarkable advantage in using graphene for realizing delay lines is related to a faster tuning condition due to the electro-optic approach, because τ_g can be quickly and easily changed by changing the applied voltage. Therefore, the maximum value of the switching energy consumption to allow a tuning of 230 ps in the cavity has been calculated by (3) [44]:

$$E_{\text{switch}} = \frac{C}{2}\left(V_{\text{ON}}^2 - V_{\text{OFF}}^2\right). \tag{9}$$

A switching energy $E_{\text{switch}} = 49.9$ pJ has been obtained, assuming $V_{\text{ON}} = 4.53$ V and $V_{\text{OFF}} = 3.67$ V. Such performance has been calculated assuming $\varepsilon_{\text{Al2O3}} = 10$, $s = 10$ nm, and an area of the electrodes $A \sim 4R^2 = 1600$ μm^2. The capacitance $C = (\varepsilon_{\text{Al2O3}} \cdot \varepsilon_0 \cdot A)/s$ resulted equal to 14 pF. A strong decrease of the capacitance $(C = 0.97$ pF$)$ has been evaluated by modifying the pattern of the electrodes; therefore, covering with the graphene layers only the microring resonators with an area of 110 μm^2. A very low energy switching consumption $E_{\text{switch}} = 3.4$ pJ has been calculated in this last case.

We have also evaluated the switching time, which is proportional to the $R_{es}C$ constant $(t_{\text{switch}} \sim R_{es}C)$ [45]. Typical experimental values of the resistance of graphene layers used as electrodes with applied voltage $V_g < 5$ V, are $R_{es} < 2$ kΩ [46]. Assuming $C = 0.97$ pF calculated when the graphene layers cover only the microrings, a switching time $t_{\text{switch}} < 2$ ns has been obtained, as reported in Table 1, that can be further optimized with lower values of resistance. This value of t_{switch} is higher than that in [20], but it is four orders of magnitude less than the typical switching time of the thermo-optically tunable optical delay lines.

The performance of the graphene-based optical delay line has been compared with the state-of-the-art of the integrated optical delay lines, as shown in Table 2. The ratio between the tuning

TABLE 2

Comparison of the performance of the graphene-based resonant cavity with the state-of-the-art of the integrated optical delay lines

Configuration	Footprint (A) [μm^2]	Delay time (τ_g) [ps]	Tuning range ($\Delta\tau_g$) [ps]	FOM ($\Delta\tau_g$/A) [ps/ μm^2]	Tuning effect	Switching Time (t_s) [ns]
SCISSOR [14]	10^8	1200 ps	1200 ps	1.2×10^{-5}	-	-
SCISSOR [12]	9×10^4	500 ps	-	-	-	-
CROW [11]	$5\cdot10^6$	800 ps	800 ps	1.6×10^{-4}	-	-
SCISSOR [16]	1.4×10^4	300 ps	300 ps	2.5×10^{-2}	Thermo-optically	> 10^4 ns
PhC [19]	2×10^5	216 ps	200 ps	10^{-3}	-	-
SCISSOR [20]	10^4		345 ps	3.4×10^{-2}	Thermo-optically	10^4 ns
Graphene-based SCISSOR [31]	< 10^5	250 ps	-	~2×10^{-3}	Electro-optically	0.12 ns
Graphene-based CROW [31]	< 10^5	200 ps	-	~2×10^{-3}	Electro-optically	0.12 ns
This work	1.6×10^3	360 ps	230 ps	1.4×10^{-1}	Electro-optically	2 ns

range and the device footprint represents an important figure of merit (FOM) for optical delay lines. A value of FOM equal to 1.4×10^{-1} ps/μm^2 has been calculated for the graphene-based cavity, which is higher of about a factor 4 compared to the values obtained by CROW configurations [16], [20], also providing a switching time several times faster and confirming the suitability of the graphene-based resonant cavity as optical delay line.

4. Conclusion

An efficient optical delay line having a very innovative configuration with high delay time up to $\tau_g = 360$ ps, broad tuning range $\Delta\tau_g = 230$ ps, bandwidth of a few GHz, $ER \leq 23$ dB, fast tunability ($t_{\text{switch}} \sim 2$ ns), low energy consumption ($E_{\text{switch}} \sim 3.4$ pJ), and very small footprint ($A = 1600\ \mu\text{m}^2$) has been designed. The achieved results demonstrate an enhancement of the figure of merit FOM $= \Delta\tau_g/A (= 1.4 \times 10^{-1}$ ps/μm$^2)$ of a factor 4 compared to the state-of-the-art of the optical delay lines also with a much faster tunability. Such performance confirms the advantage of the graphene integration in the resonant optical devices to obtain an efficient light modulation and the suitability of the graphene-based resonant cavity as optical delay line for several applications, mainly for fast beam steering of phased array antennas in optical beamformers, because it fully satisfies the requirements of a switching time under 10 μs and $\Delta\tau_g > 200$ ps [17].

References

[1] G. Lenz, B. J. Eggleton, C. K. Madsen, and R. E. Slusher, "Optical delay lines based on optical filters," *IEEE J. Quantum Electron.*, vol. 37, no. 4, pp. 525–532, Apr. 2001.

[2] H. Park, J. P. Mack, D. J. Blumenthal, and J. E. Bowers, "An integrated recirculating optical buffer," *Opt. Exp.*, vol. 16, no. 15, pp. 11124–11131, Jul. 2008.

[3] Y. Liu, J. Yang, and J. Yao, "Continuous true-time-delay beamforming for phased array antenna using a tunable chirped fiber grating delay line," *IEEE Photon. Technol. Lett.*, vol. 14, no. 8, pp. 1172–1174, Aug. 2002.

[4] L. Zhuang *et al.,* "Novel ring resonator-based integrated photonic beamformer for broadband phased array receive antennas—Part I: Design and performance analysis," *IEEE J. Lightw. Technol.*, vol. 28, no. 1, pp. 3–18, Jan. 2010.

[5] X. Ye, F. Zhang, and S. Pan, "Optical true time delay unit for multibeamforming," *Opt. Exp.*, vol. 23, no. 8, pp. 10002–10008, Apr. 2015.

[6] R. L. Moreira *et al.,* "Integrated ultra-low-loss 4-bit tunable delay for broadband phased array antenna applications," *IEEE Photon. Technol. Lett*, vol. 25, no. 12, pp. 1165–1168, Jun. 2013.

[7] J. Xie, L. Zhou, Z. Li, J. Wang, and J. Chen, "Seven-bit reconfigurable optical true time delay line based on silicon integration," *Opt. Exp.*, vol. 22, no. 19, pp. 22707–22715, Sep. 2014.

[8] B. Vidal, T. Mengual, C. Ibáñez-López, and J. Marti, "Optical beamforming network based on fiber-optical delay lines and spatial light modulators for large antenna arrays," *IEEE Photon. Technol. Lett.*, vol. 18, no. 24, pp. 2590–2592, Dec. 2006.

[9] H. Lee, T. Chen, J. Li, O. Painter, and K. J. Vahala, "Ultra-low-loss optical delay line on a silicon chip," *Nature Commun.*, vol. 3, pp. 1–7, May 2012.

[10] J. K. S. Poon, J. Scheuer, Y. Xu, and A. Yariv, "Designing coupled-resonator optical waveguide delay lines," *J. Opt. Soc. Amer. B*, vol. 21, pp. 1665–1673, 2004.

[11] F. Morichetti, C. Ferrari, A. Canciamilla, and A. Melloni, "The first decade of coupled resonator optical waveguides: Bringing slow light to applications," *Laser Photon. Rev.*, vol. 6, no. 1, pp. 74–96, Jan. 2012.
[12] F. Xia, L. Sekaric, and Y. Vlasov, "Ultracompact optical buffers on a silicon chip," *Nature Photon.*, vol. 1, pp. 65–71, 2007.
[13] W. Bogaerts *et al.,* "Silicon microring resonators," *Laser Photon. Rev.*, vol. 6, no. 1, pp. 47–73, Jan. 2012.
[14] L. Zhuang *et al.,* "Single-chip ring resonator-based 1 $\times$ 8 optical beam forming network in CMOS-compatible," *IEEE Photon. Technol. Lett.*, vol. 19, no. 15, pp. 1130–1132, Aug. 2007.
[15] A. Craig Beal, P. D. Kumavor, J. H. Kelrn, and B. C. Wang, "Fast tunable parallel optical delay line for multi-rate communication and dynamic bandwidth allocation," in *Proc. IEEE 17th Annu. Meet. Lasers Electro-Opt. Soc.*, 2004, pp. 709–710.
[16] F. Shinobu, N. Ishikura, Y. Arita, T. Tamanuki, and T. Baba, "Continuously tunable slow-light device consisting of heater-controlled silicon microring array," *Opt. Exp.*, vol. 19, no. 4, pp. 13557–13564, Jul. 2011.
[17] T. Baba, "Slow light in photonic crystals," *Nature Photon.*, vol. 2, pp. 465–473, 2008.
[18] H. Tian, F. Long, W. Liu, and Y. Ji, "Tunable slow light and buffer capability in photonic crystal coupled-cavity waveguides based on electro-optic effect," *Opt. Commun.*, vol. 285, no. 10/11, pp. 2760–2764, May 2012.
[19] C.-Y. Lin *et al.,* "Silicon nanomembrane based photonic crystal waveguide array for wavelength-tunable true-time-delay lines," *Appl. Phys. Lett.*, vol. 101, 2012, Art. ID 051101.
[20] P. A. Morton, J. Cardenas, J. B. Khurgin, and M. Lipson, "Fast thermal switching of wideband optical delay line with no long-term transient," *IEEE Photon. Technol. Lett.*, vol. 24, no. 6, pp. 512–514, Mar. 2012.
[21] K. Geim and K. S. Novoselov, "The rise of graphene," *Nature*, vol. 6, pp. 183–191, 2007.
[22] F. Bonaccorso, Z. Sun, T. Hasan, and A. C. Ferrari, "Graphene photonics and optoelectronics," *Nature Photon.*, vol. 4, pp. 611–622, 2010.
[23] C. Qiu *et al.,* "Efficient modulation of 1.55 μm radiation with gated graphene on a silicon microring resonator," *Nano Lett.*, vol. 14, pp. 6811–6815, 2014.
[24] C. T. Phare, Y.-H. D. Lee, J. Cardenas, and M. Lipson, "Graphene electro-optic modulator with 30 GHz bandwidth," *Nature Photon.*, vol. 9, pp. 511–514, 2015.
[25] T. H. Han *et al.,* "Extremely efficient flexible organic light-emitting diodes with modified graphene anode," *Nature*, vol. 6, pp. 105–110, 2012.
[26] K. S. Novoselov *et al.,* "A roadmap for graphene," *Nature*, vol. 490, no. 7419, pp. 192–200, 2010.
[27] T. Pan *et al.,* "Analysis of an electro-optic modulator based on a graphene-silicon hybrid 1D photonic crystal nanobeam cavity," *Opt. Exp.*, vol. 23, no. 18, pp. 23357–23364, Sep. 2015.
[28] Y. Song *et al.,* "Role of interfacial oxide in high-efficiency graphene—Silicon Schottky barrier solar cells," *Nano Lett.*, vol. 15, no. 3, pp. 2104–2110, Mar. 2015.
[29] A. Majumdar, J. Kim, J. Vuckovic, and F. Wang, "Electrical control of silicon photonic crystal cavity by graphene," *Nano Lett.*, vol. 13, no. 2, pp. 515–518, Feb. 2013.
[30] J. K. Thind, M. Kumar, and B. K. Kaushik, "Electrical tuning of optical delay in graphene-based photonic crystal waveguide," *IEEE J. Quantum Electron.*, vol. 51, no. 10, Oct. 2015, Art. ID 6400105.
[31] J. Capmany, D. Domenech, and P. Munoz, "Silicon graphene reconfigurable CROWS and SCISSORS," *IEEE Photon. J.*, vol. 7, no. 2, Apr. 2015, Art. ID 7050244.
[32] J. L. Zhuang *et al.,* "Phased array receive antenna steering system using a ring resonator-based optical beam forming network and filter-based optical SSB-SC modulation," in *Proc. IEEE Int. Topical Meet. Microw. Photon.*, Victoria, BC, Canada, 2007, pp. 88–91.
[33] C. Rosa, J. Rogers, and A. G. Podoleanu, "Fast scanning transmissive delay line for optical coherence tomography," *Opt. Lett.*, vol. 30, no. 24, pp. 3263–3265, Dec. 2005.
[34] A. Gondarenko, J. S. Levy, and M. Lipson, "High confinement micron-scale silicon nitride high Q ring resonator," *Opt. Exp.*, vol. 17, no. 14, pp. 11366–11370, Jul. 2009.
[35] C. Ciminelli, D. Conteduca, F. Dell'Olio, and M. N. Armenise, "Novel graphene-based photonic devices for efficient light control and manipulation," in *Proc. IEEE ICTON*, Budapest, Hungary, 2015, pp. 1–4.
[36] C. Ciminelli, C. E. Campanella, F. Dell'Olio, and M. N. Armenise, "Fast light through velocity manipulation in two vertically-stacked ring resonators," *Opt. Exp.*, vol. 18, no. 3, pp. 2973–2986, Feb. 2010.
[37] C. A. Barrios *et al.,* "Demonstration of slot-waveguide structures on silicon nitride/silicon oxide platform," *Opt. Exp.*, vol. 15, no. 11, pp. 6846–6856, May 2007.
[38] K. Preston, B. Schmidt, and M. Lipson, "Polysilicon photonic resonators for large-scale 3D integration of optical networks," *Opt. Exp.*, vol. 15, no. 25, pp. 17283–17290, Dec. 2007.
[39] E. Simsek, "A closed-form approximate expression for the optical conductivity of graphene," *Opt. Lett.*, vol. 38, no. 9, pp. 1437–1439, May 2013.
[40] V. Sorianello, M. Midrio, and M. Romagnoli, "Design optimization of single and double layer graphene phase modulators in SOI," *Opt. Exp.*, vol. 23, no. 9, pp. 6478–6490, Mar. 2015.
[41] Z. Lu and W. Zhao, "Nanoscale electro-optic modulators based on graphene-slot waveguides," *J. Opt. Soc. Amer. B*, vol. 29, pp. 1490–1496, 2012.
[42] F. Dell'Olio, D. Conteduca, C. Ciminelli, and M. N. Armenise, "New ultrasensitive resonant photonic platform for label-free biosensing," *Opt. Exp.*, vol. 23, pp. 28593–28604, 2015.
[43] R. C. Alferness and P. S. Cross, "Filter characteristics of codirectionally coupled waveguides with weighted coupling," *IEEE J. Quantum Electron.*, vol. QE-14, no. 11, pp. 843–847, Nov. 1978.
[44] M. Midrio *et al.,* "Graphene—Assisted critically—Coupled optical ring modulator," *Opt. Exp.*, vol. 20, pp. 23144–23155, 2012.
[45] J. Gosciniak and D. T. H. Tan, "Theoretical investigation of graphene-based photonic modulators," *Sci. Rep.*, vol. 3, 2013, Art. ID 1897.
[46] X. Li *et al.,* "Transfer of large-area graphene films for high-performance transparent conductive electrodes," *Nano Lett.*, vol. 9, pp. 4359–4363, 2009.